# Computational Modeling of 2D Mangrove Forests for Scour Mitigation around Bridge Piers

by

Andrew Carl Enns

A Dissertation Presented in Partial Fulfillment
of the Requirements for the Degree
Master of Science

Approved June 2021 by the
Graduate Supervisory Committee:

Leon van Paassen, Co-Chair
Junliang Tao, Co-Chair
Edward Kavazanjian

ARIZONA STATE UNIVERSITY

August 2021

ABSTRACT

Bridge scour at piers is a major problem for design and for maintaining old infrastructure. The current methods require their own upkeep and there may be better ways to mitigate scour. I looked to the mangrove forests of coastal environments for inspiration and have developed a 2D model to test the efficacy of placing a mangrove-root inspired system to mitigate scour. My model tests the hydrodynamics of the root systems, but there are additional benefits that can be used as bioinspiration in the future (altering the surrounding chemistry and mechanical properties of the soil).

Adding a mangrove inspired minipile system to bridge piers changes scour parameters within my 2D COMSOL models. For the volume of material added, the minipiles compare favorably to larger sacrificial piles as they reduce $A_{wcz}$ and $\tau'_{max}$ by similar (or even better) amounts. These two parameters are indicators of scour in the field. Within the minipile experiments, it is more beneficial to place them upstream of the main bridge pier as their own 'mangrove forest.' The value of $A_{wcz}$ and $\tau'_{max}$ for complex 2D models of scour is unclear and physical experiments need to be performed. The model geometry is based on the dimensions of the experimental flume to be used in future studies and the model results have not yet been verified through experiments and field trials. Scale effects may be present which cannot be accounted for in the 2D models. Therefore future work should be conducted to test 'mangrove forest' minipile systems in 3D space, in flume experiments, and in field trials.

# DEDICATION

This work is dedicated to my family and friends for their continued support and guidance throughout my time at ASU.

ACKNOWLEDGMENTS

The presented study involves work primarily supported by the Engineering Research Center Program of the National Science Foundation under NSF Cooperative Agreement No. EEC-1449501. Any opinions, findings, and conclusions or recommendations expressed in this material are those of the author(s) and do not necessarily reflect those of the National Science Foundation.

Several people have contributed to my time learning at ASU. These include many of the professors and students within the Center for Bio-mediated and Bio-inspired Geotechnics (CBBG). Dr. Kavazanjian, Dr. Houston, and Dr. Zapata all taught me a lot more about the soil below my feet (and buildings!) than I had ever stopped to think about before. Dr. van Paassen and Dr. Tao were both essential to this work and to helping me navigate my way from strictly geology to a more engineering point of view. The students of CBBG as well were a font of knowledge and great friends. Thank you each to Miriam, Austin, Pancho, Robin. Thank you to Preston Wong, Xiwei Li, and Joel Ramirez for contributing towards the following work as well.

I would like to thank all my friends for contributing to my sanity and encouraging me to finish- Mike Veto, Jean-Francois Smekens and Allie Rutledge, Mike Pagano, Scott Dickenshied, Pilar Vergeli and Tucker Dunn, Natalie Hinkel and Caleb Wheeler, Andy Ryan, Barret Salsibury, and so many more. Whether you were part of SESE, CBBG, or my undergraduate work: thank you.

My family has been so supportive during my education. Mom and Dad, Kyle, Kevin, and Haley I love you all and look forward to when we can visit more easily post-COVID19. Lastly I

could never have finished without the love and support of Aleisha Johnson who has always pushed me to do my best and be myself.

TABLE OF CONTENTS

Page

LIST OF TABLES

Table Page

LIST OF FIGURES

Figure Page

FIGURE Page

LIST OF SYMBOLS

| | |
|---|---|
| $v$ | Flow velocity, m/s |
| $v_c$ | Critical flow velocity, m/s |
| $K_s$ | Shields parameter |
| $S_s$ | Specific gravity of sediment/bed material |
| $D_{50}$ | Median size of bed material, m |
| $y$ | Depth of flow, m |
| $n$ | Manning roughness coefficient |
| $\tau$ | Bed shear stress, $Pa = kg/ms^2$ |
| $\tau_c$ | Critical bed shear stress, $Pa = kg/ms^2$ |
| $\tau'$ | Normalized shear stress |
| $y_s$ | Scour depth, m |
| $y_1$ | Flow depth, m |
| $K_1$ | Correction factor for pier nose shape |
| $K_2$ | Correction factor for angle of attack of flow |
| $K_3$ | Correction factor for bed condition |
| $a$ | Pier width, m |
| $Fr$ | Froude Number = $V/\sqrt{gy_1}$ |
| $g$ | Acceleration due to gravity, 9.81 m/s$^2$ |
| $D$ | Pier diameter, m |
| $d$ | Minipile diameter, ~1% of D, m |

$T_w$ Topwidth of scour hole, m

$X$ Distance between furthest upstream minipile and the center of the main pile

$\alpha$ Wedge angle, °

$RR_{50}$ Median size of rip rap, m

$K_{RR}$ Correction factor for rip rap

$S_{RR}$ Specific gravity of rip rap

$\rho_w$ Density of water, kg/m$^3$

# Chapter 1

# INTRODUCTION

## 1.1 Scour Overview

Scour drives erosion around structures built in active flow regimes (e.g. hydraulic environments). Soil and sand particles around the foundation base at the sand/water boundary will be displaced and reduce the efficacy of the foundation system. In turn this drives either more expensive material costs to account for a deeper foundation or failure in structures that were not designed with scour in mind. The National Cooperative Highway Research Program (NCHRP) reported that during the time span from 1966-2005, 58% of reported bridge failures (1,502 in total) in the United States were attributed to scour (Hunt 2009).

Scour then has to be accommodated in design so that foundation systems do not fail. Scour countermeasures commonly used in practice, along with their design guidelines, are included in the Hydraulic Engineering Circular (HEC) No. 23 (Lagasse et al. 2009) and No. 18 (Arneson et al. 2012) for bridges and in Offshore Standard DNV-OS-J101 (DNV 2010) for offshore wind turbines. However, these countermeasures are subject to their own service life limitations and require periodic inspection, increasing the costs and risks over time. Scour countermeasures can even fail on their own (Lagasse et al. 2009; Sumer and Nielsen 2013). Thus researchers continue to seek more robust and cost-effective scour countermeasures. As climate change actively drives a more intense

storm environment (source?) and increasing interests in offshore wind energy it is necessary to develop new sustainable, cost effective, and easy to implement scour countermeasures.

So how big of a problem is scour now? Most bridges were not designed with scour in mind prior to 1991 (USDOT 1988, Arneson et al. 2012). Bridges were instead built to differing design standards with 70% not required to account for scour or designed for less extreme precipitation events (Flint et al. 2017). While Hunt (2009) found 58% of bridge failures attributed to scour, newer studies see lower scour failures over more recent years. From 1987-2011 scour accounted for 19% (n=131) of failures (Cook 2014). These numbers seem optimistic, but they also purposefully don't include other hydraulic failures during large precipitation events. While scour may not be the primary driver of bridge failure during floods or otherwise high flows it undoubtedly lowers a bridge's ability to survive the event. Scour then is a large hazard for older bridges and still a major failure mode for design of new bridges.

## 1.2 Scour Mitigation

Current solutions to mitigate scour are described in the FEH manual (ref) and have been implemented in bridge designs after 1991. These methods include utilizing rip rap covers and sacrificial piles. The mechanism of scour mitigation for each method is different. Riprap involves placement of aggregate stone on the flow bed, which because of their larger grain size increases the shear resistance of the flow bed. Sacrificial piles

are placed upstream from the main pile foundation and reduce the shear force at the main foundation. Current engineered solutions to mitigate scour require a significant amount of materials and energy for construction and maintenance and have significant environmental impact. As an alternative, nature also provides solutions to mitigate scour. For example, mangrove forests, seagrass, and coral reefs all provide scour protection to their environments (Guannel et al. 2016). Mangroves interact with soil in several ways. Broadly these interactions can be broken into three categories:

1. Hydrodynamic – roots disrupt the flow and dampen flow energy, reducing the shear force (Chen 2012, Kazemi 2017, Tomiczek 2020).
2. Mechanical – root reinforcement of soil and water uptake/removal from soil, increasing shear resistance (Waldron 1977, Ola 2015).
3. Chemical – root and microbe exudates and chemical products, and decay of organic matter, increasing shear resistance (Mendoza 2007, Andrade 2012).

One of the best studied rhizospheres is that of the mangrove tree common to the tropic and subtropic coasts. Perhaps most visibly, mangrove forests protect coastlines from erosion thanks to their complex root systems (Adame 2010, Guannel 2016). The mangrove root structures trap sediment and encourage deposition in some cases (Adame 2010). At the same time, some mangrove species have complex rhizospheres that cause precipitation of inorganic minerals (pyrite), which may consolidate the sediments and increase shear resistance (Mendoza 2007, Andrade 2012). It is unclear if the pyrite causes any increase in shear strength of the soil as the authors were most interested in the water geochemistry and the sediments as a deposit of heavy metals. The microbes and fungi within the mangrove

rhizosphere then at least have potential for environmental engineering practice to clean up heavy metals.

The objectives of this study are to learn about the benefits that mangrove forests provide to their environment and to translate them to submerged bridge and mono-pile foundation systems. This study focuses on the hydromechanical aspects. My focus in this work is to adapt the mechanical aspects of the mangrove root systems to that of hydraulic pile foundations.

## 1.3 This Work

I propose that I can significantly reduce the effects of scour on a monopile system by mimicking aspects of mangrove forests. Specifically I will leverage the many roots present on a mangrove tree to reorient/redistribute the water flow velocities and shear stresses at the base of the monopile to discourage the effects of scour. Because approach flow velocity is positively correlated with scour depth (Unger and Hager 2007) any reduction in flow velocity will reduce scour as well as the resultant force on a monopile (Tomiczek 2020).

Our goals then are to reduce, through clever/novel use of mangrove inspired design, the parameters that influence the ultimate scour depth of a bridge pier system. To test my hypothesis I will start by modeling unique geometries around monopile systems within the COMSOL Multiphysics software package. My initial scope is to explore these

systems in a 2-dimensional analysis before proceeding towards 3D models and experimental flume studies with the best geometries I uncover.

# Chapter 2

# LITERATURE REVIEW

## 2.1 Local Scour

Scour will occur any time a river flow must divert around a structure (generally bridge piers and abutments) and the shear stress, $\tau$, the flow imparts on the bed surface exceeds the critical shear stress, $\tau_c$. Shear stress in the system is related to the flow parameters in Eq 2.1:

$$\tau = \rho_w v^2 \tag{2.1}$$

Because the density of water, $\rho_w$, is constant, any changes in the flow velocity caused by an emplaced structure can push the flow velocity above some critical velocity, $v_c$, to initiate grain transport. There are many empirical equations for critical velocity, but the one that I will use in this document is described in Appendix C of the HEC 18:

$$v_c = \left[\frac{K_s^{1/2}(S_s - 1)^{1/2} D_{50}^{1/2} y_1^{1/6}}{n}\right] \tag{2.2}$$

Using $K_s = 0.039$, $S_s = 2.65$, and $n = 0.041 D_{50}^{1/6}$

$$v_c = 6.19 y_1^{1/6} D_{50}^{1/3} \quad (2.3)$$

Then when $v$ is above $v_c$, scour will occur. But what does the initiation of scour look like?

As a pier or abutment impedes flow, water is redirected around the structure. Water that is directed downward will form horseshoe vortices when they next interact with the riverbed. A scour hole develops as the transport rate of sediment away from the base overcomes the transport rate around the base. As the scour hole grows, these rates move closer to each other until they reach equilibrium and the scour hole reaches its final size. In clear-water scour conditions, the scour will reach equilibrium when the shear stress, $\tau$, imparted onto the bed by the horseshoe vortex is equal to the critical shear stress of the sediment particles, $\tau_c$ within the scour hole. The scour develops in 4 (Unger and Hager 2007, Figure 2.1):

I. An initial vortex forms in the center of the channel (the channel symmetry axis) and entrains sediment from the pier sides. Scour develops along these side pathways.
II. The initial vortex fades after the scour holes migrate to the channel symmetry axis.
III. A scour inducing single horseshoe vortex develops in the scour hole. Flow inside the scour hole is always attached to the pier.

IV. A mature horseshoe vortex system develops with primary and possibly one or more secondary vortices. Maximum scour depth migrates to the leading pier front. Scour hole extension drives subsequent decrease in flow velocity around pier and deceleration of scour advance. No flow separation from pier at bed surface.

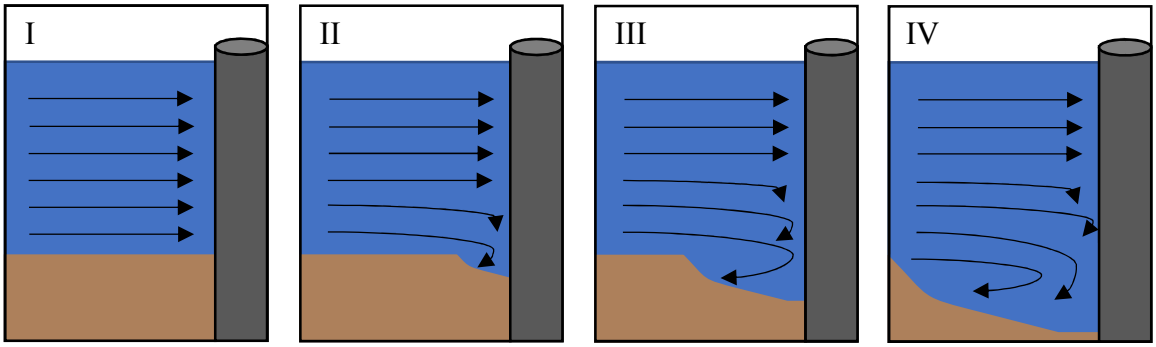


**Figure 2.1** Sketch of scour development in front of a bridge pier showcasing the 4 distinct stages.

The size of the final scour hole can be calculated either as an equilibrium scour (Arneson 2012) or as time-dependent (Unger and Hager 2007). The size of the scour hole is influenced by the parameters of the river and the structure built over it: (1) the approach flow velocity, $v$, (2) the flow depth, $y_1$, (3) the pier width, (4) the length of the pier, (5) the bed material, (6) approach flow angle of attack, (7) pier shape, (8) bed configuration, and (9) debris within the system (Arneson 2012, Richardson and Davis 2001, Tao 2013, Li 2018).

The HEC 18 recommends an empirical equilibrium equation developed by researchers at Colorado State University (Richardson and Davis 2001, Shen et al. 1966, Molinas 2001, Melville and Sutherland 1988):

$$\frac{y_s}{a} = 2.0K_1K_2K_3\left(\frac{y_1}{a}\right)^{0.35}Fr^{0.43} \quad (2.4)$$

This equation is versatile in that it can be rearranged to describe scour depth, $y_s$, as a function of any of the variables noted above, though primarily as a function of flow depth, $y_1$. The various correction factors and how they vary can be found within Chapter 7 of the HEC 18. The CSU equation is generally recommended for design as it rarely underpredicts the scour depth (Mueller 1996). When you can calculate your anticipated scour, you can then start designing systems to account for and mitigate the scour.

## 2.2 Quantifying Scour Mitigation

Scour mitigation works from one of two angles: (1) change the critical velocity required for scour to do the most damage, and (2) change the flow characteristics around the bridge structure. Riprap works primarily to increase the critical velocity needed by adding large aggregate as an armor for the base bed material. HEC 23 Vol I describes the standard method for sizing your riprap:

$$RR_{50} = \frac{0.692(K_{RR}v)^2}{\left(2g(S_{RR}-1)\right)} \quad (2.5)$$

At the same time, riprap is also prone to its own failure mechanisms under clear water conditions: Shear failure, Winnowing failure, and Edge failure (Chiew 1995, HEC 23).

Riprap can fail to the same shear stresses as normal sediment if not designed for appropriate downflow and horseshoe vortex forces around the bridge pier. The material underlying the layer of riprap can be winnowed away if there are large enough voids in the riprap layer. Finally scour around the edge of the riprap layer instead and can eventually creep towards the bridge pier. Further under live-bed conditions scour is also vulnerable to bedform-induced and bed-degredation induced failues as bedforms or scour change the amount of support available to the riprap (Chiew 2002).

Sacrificial piles work to change the flow characteristics and reduce shear stresses and velocities around the load bearing bridge piers. Flume experiments by Melville and Hadfield (1999) see that sacrificial piles reduce scour for aligned and low intensity flows. They tested a range of geometries to find the best performance but conclude that sacrificial piles should not be the primary method for mitigating scour.

## 2.3 Previous Work on Mangrove Morphology

Physical models tend to explore the interactions between obstacles in a flow path and the flow parameters that develop around them (Melville and Hadfield 1999, Kazemi et al. (2017), Chen et al. (2012), and Tomiczek et al. (2020) were all done with various hydraulic setups and different physical models.

Chen et al. (2012) looked to analyze the mean and turbulent flow structure in the wake of a patch of vegetation. Using an experimental flume, they used a circular array of cylinders to model different ‘porosities’ of vegetation. They found and modeled

relationships between the array size and porosity with the flow velocity as it exited the array. From this they also predicted regions of deposition behind their porous array.

In an effort to determine how mangrove roots influence the flow structure of surrounding water, Kazemi et al. (2017) used an experimental flume to explore the effects of 'porous' barriers on flow parameters (Re, Cd, applied force, Strouhal number [St]). They inserted a model, fixed to the surface at the top of their flume, and varied the model geometry and flexure as well as the input flow velocity. The study finds that more tightly packed (less porous) barriers act more like a larger singular cylinder to the flow as well as that flexible root structures (that can bend to the flow itself) aid in creating a lower velocity zone behind the root system.

Tomiczek et al. (2020) use an array of model mangroves to explore their effect on wave motions and forces transmitted to structures they are protecting. This work focuses more on how waves interact with the mangrove structure above and below water-level than how mangroves interact with a constant current. Increasing the cross-sectional area mangroves interacted with the wave motions caused a reduction in peak water velocities and forces transmitted to the structures.

Importantly, none of the physical model systems attempt to directly describe how these systems affect the local scour. At best they make inferences based on velocity (Chen 2012). They do however have some important implications that flexible mangrove patches of a certain porosity/cross-sectional area can reduce flow velocity and force behind the systems (Kazemi 2017, Tomiczek 2020).

## 2.4 Computational Studies

Khosronejad et al (2012) use Computational Fluid Dynamics (CFD) to explore how three bridge pier shapes affect local scour. They use software of their own design that uses unsteady Reynolds averaged Navier Stokes (URANS) with a k-w turbulence closure for the fluid/hydrodynamics calculations coupled to a sediment continuity equation to model the fluid-structure/bed surface interactions. Their Study was coupled with an experimental flume where they found that their URANS model underpredicted scour for 'blunt-edged' bridge piers.

Tao (2013) used CFD to investigate the effect of pier shape, aspect ratio, and attack angle on scour formation. They find that pier shapes will affect downward flow fluid and can be manipulated to weaken said flow. Combining simulated flows with scour patterns also find that maximum bed shear stress correlates with the maximum scour depth locations though this does not necessarily indicate the depth of scour. Li (2018) explored how streamlining piers could reduce the effects of scour. They model, in 3D, different streamlined piers and analyze the modified flow intensity. Li (2018) uses weighted critical zone areas and maximum normalized shear stresses within their model for this analysis.

While there are several studies (Khosronejad et al. 2012, Tao 2013, Li 2018) that use CFD to investigate scour around bridge piers, there are no current numerical simulations for how a 'porous' system would relate to bed shear stress around a central bridge pier.

# Chapter 3

# METHODS

*'The map is not the territory'*

*Or*

*'All models are wrong'*

## 3.1 COMSOL Multiphysics

I use COMSOL Multiphysics (hereafter COMSOL) to model my system. COMSOL is a Finite Element Method that can simulate a variety of different physics and chemistries separately or coupled. I use COMSOL as a way to explore Computational Fluid Dynamics (CFD) for my imagined system.

I believe COMSOL to be a valid form of study as it has been used previously in Tao (2013) and Li (2018) to examine through CFD the role of the shape of the monopile to incipient scour. Kazemi et al. (2017) used an experimental flume to examine the effect of porous root-like systems on flow parameters. My efforts are to combine these previous CFD studies with results from experimental flumes and test my different geometries within COMSOL. Then use these model outputs to inform future 3D COMSOL models as well as tests done within an experimental flume.

Within COMSOL, I use a kappa-omega (k-w) turbulence model to calculate velocities in my model. *Explanation of k-w turbulence model*. COMSOL was configured

with a Reynolds-Averaged Navier Stokes (RANS) approach with a $k$-ω approximation to model the turbulence. RANS models steady state flow for a turbulent system and satisfies the following equations that express flow characteristics as functions of the coordinates, independent of time:

$$\begin{cases} \dfrac{d\bar{u}_i}{dx_i} = 0 \\ \bar{u}_j \dfrac{d\bar{u}_j}{dx_j} = -\dfrac{1}{\rho}\dfrac{\partial \bar{p}}{\partial x_i} + v\dfrac{\partial^2 \bar{u}_i}{\partial x_j x_j} + \bar{f_i} - \dfrac{\partial \overline{u_i' u_j'}}{\partial x_j} \end{cases} \tag{3.1}$$

The calculations resolve into a mean flow with fluctuating turbulent components. This has implications for how flow velocity impacts the bed shear stresses seen in physical systems. As per the norm for turbulent flow, the walls on the model are set to no-slip surfaces.

## 3.2 Model Setup

For these initial stages, I use a 2D model of a mini-piles in different geometry setups around a larger singular monopile. 2D models have the advantage of being computationally simple and thus converge more quickly to a solution and enable exploring more parameter space.

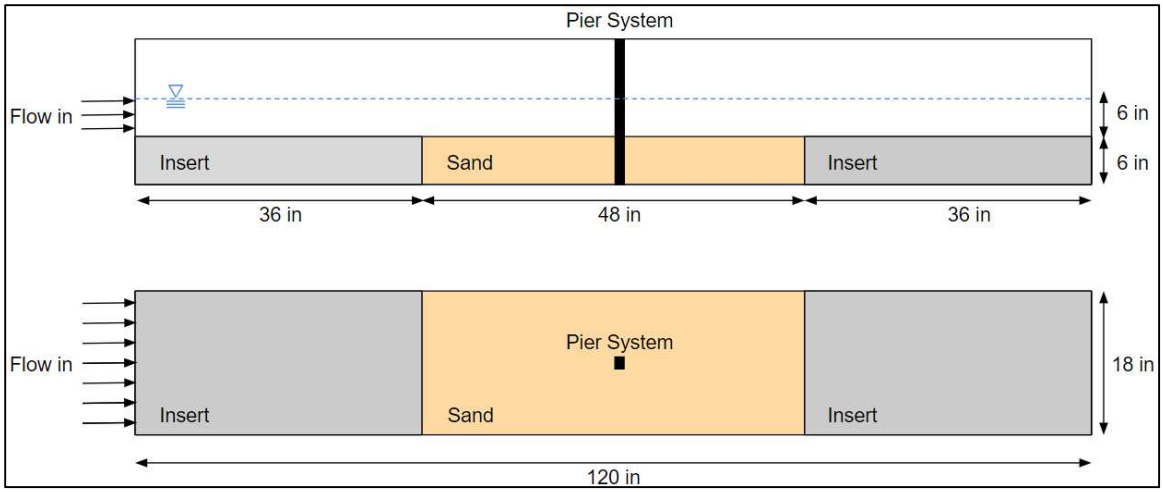


**Figure 3.1** Expected ISTB4 flume setup for measuring scour around a central pier and mini-pile system. Water inflow at a set velocity travels through the flume and interacts with the sand around the pier system.

Future physical experiments will be done in an experimental flume located in the ISTB4 building of the ASU Tempe Campus (Figure 3.1). Dimensions of the flume are used for dimensions within the COMSOL model. $D_{50}$ of the sediment on hand was measured (Figure 3.2) and then used to calculate the critical velocity with Eq. 2.2. The input velocity of the model is set to ~90% of the critical velocity as used in other investigations of clear water scour (Unger and Hager 2007). Initial conditions and dimensions used for all COMSOL models are listed in Table 3.1. Mini-pile diameter is set to 1% of the bridge pier diameter per my estimates of the diameter of a bamboo branch compared to a 4 to 6 m diameter bridge pier.

Table 3.1 Model constants and initial conditions

| Input Velocity | Critical Velocity | Bridge Pier Diameter | Minipile Diameter | Model length | Model width |
|---|---|---|---|---|---|
| m/s | m/s | m | mm | m | m |
| 0.3 | 0.339 | 0.046 | 0.46 | 1.2 | 0.4572 |

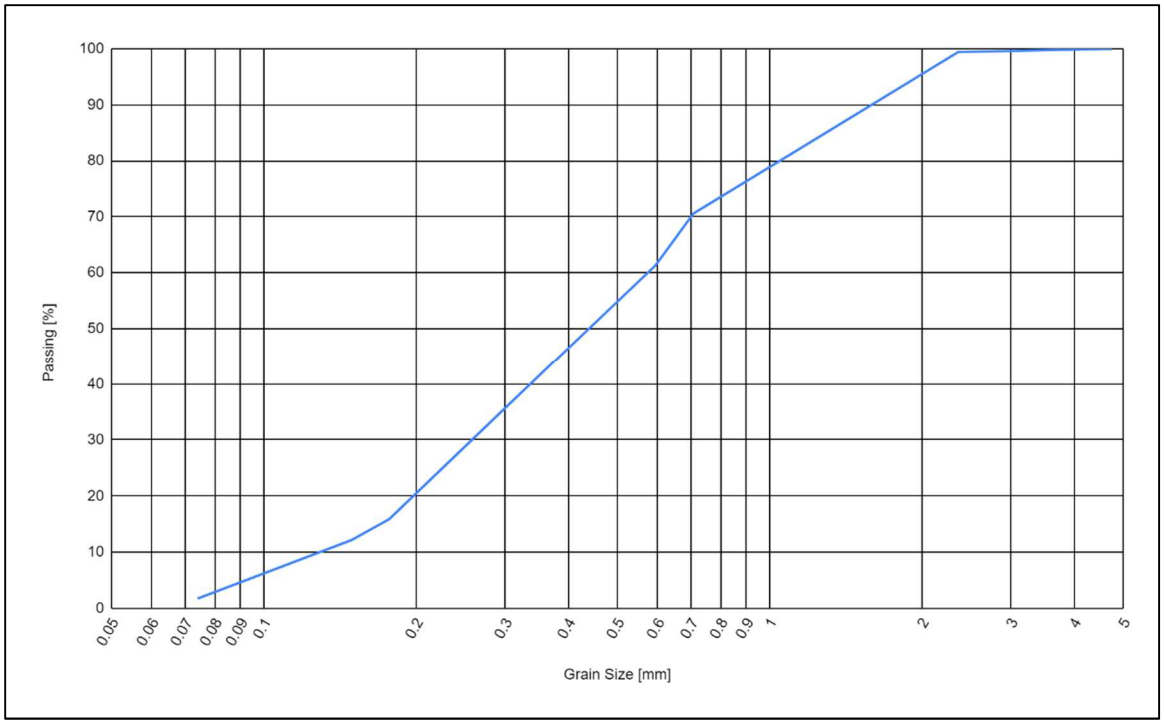


**Figure 3.2** Grain size distribution of sand used to calculate critical velocity in the system. $D_{50}$ is measured at 0.42 mm and the sand is a Well Graded Sand.

## 3.3 Geometries Investigated

Several mini-pile geometries were investigated to ascertain their benefit against the scour process: (1) Triangles, (2) Half-circles, and (3) two series of multi-layered geometries, and (4) a simple sacrificial pile. A sketch (Figure 3.3) showcases parameters used to build and modify the separate model configurations. A variety of models were build by varying x, y, α, and the number of minipiles in the system, n. The full set of experimental variance can be seen in Table 3.2.

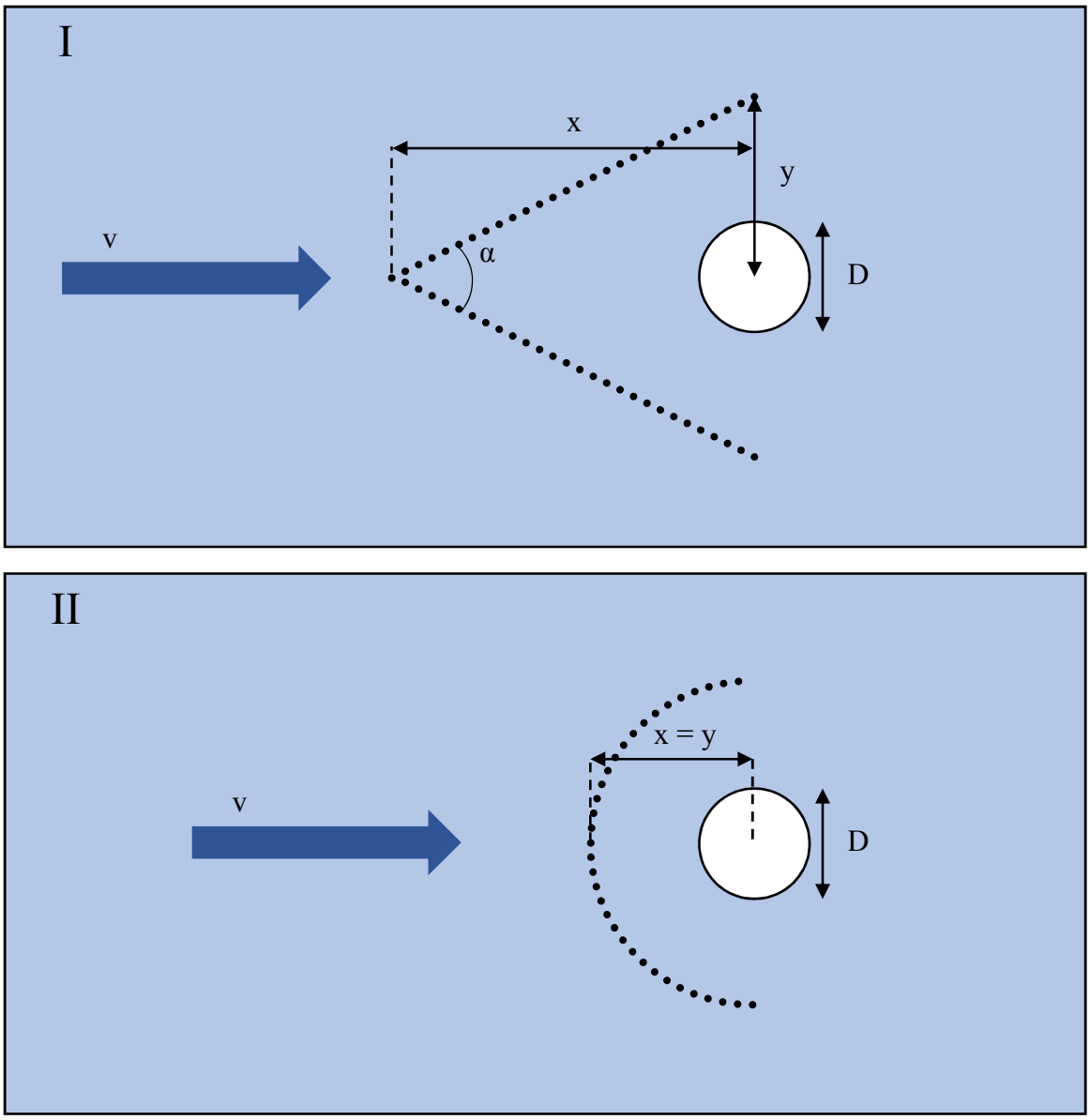


**Figure 3.3** Sketchup of two model configurations. I is a triangular minipile configuration with a wedge angle, α and the furthest minipile forward a distance x from the center of the main bridge pier. Inflow of the system is always directly upstream of the modeled system and set at a constant velocity $v = 0.9v_c$ for all model runs. II is a half-circle model.

**Triangles**. The minipiles within the triangular root system are equally spaced between themselves with the closest minipile a set center to center distance from the bridge pier (Figure 3.3). Four different wedge angles were considered: 20°, 53.6°, 90°

and 180° degrees. Triangular angles of 20° and 53.6° degrees were modeled after the sacrificial pile experiments done by Melville & Hadfield (1999). One series of models explores the effect of slowly increasing the distance x and y from the central pier. One other series modeled with triangular shapes are a set of 90° minipile systems that are placed at increasing distances upstream of the main pier. One last series of experiments does the same, but with a wedge angle of 180°-a line that is emplaced at increasing distances upstream. Table 3.2 displays the experimental setup for all triangular models.

**Half-circles.** The minipiles within the circular root system are placed as equal degree offsets from the center of the bridge pier at a set center to center distance, x=y (Figure 3.3). This series of models increases in distance from 0.55 to 1.25 diameters upstream of the main pier (Table 3.2).

**Multi-layered Minipiles.** Two sets of models were run with up to 3 different layers of minipiles. One set was done with a 90° triangular setup while the second was done with a half-circle. Experimental setups are found in Table 3.3

**Sacrificial Pile.** A sacrificial pile the same diameter as the central bridge pier was modeled at increasing upstream distance from the main pier. Table 3.4 shows the experimental setup for the models.

| Table 3.2 Experimental setups for Triangular and Half-circle COMSOL models. | | | | | |
|---|---|---|---|---|---|
| Experiment Set | Case Number | Number of Minipiles n | Wedge Angle ° | x Distance (x/D) | y Distance (y/D) |
| Triangular | 1 | 39 | 90 | 0.75 | 0.75 |
| | 2 | 41 | 90 | 0.8 | 0.8 |
| | 3 | 43 | 90 | 0.85 | 0.85 |
| | 4 | 47 | 90 | 0.9 | 0.9 |
| | 5 | 49 | 90 | 0.95 | 0.95 |
| | 6 | 51 | 90 | 1 | 1 |
| | 7 | 63 | 90 | 1.25 | 1.25 |
| | 8 | 33 | 53.6 | 1.29 | 0.65 |
| | 9 | 51 | 53.6 | 1.98 | 1 |
| | 10 | 63 | 53.6 | 2.45 | 1.25 |
| | 11 | 29 | 20 | 3.12 | 0.55 |
| | 12 | 51 | 20 | 5.67 | 1 |
| | 13 | 63 | 20 | 7.03 | 1.25 |
| | 14 | 51 | 90 | 3 | 1 |
| | 15 | 51 | 90 | 5 | 1 |
| | 16 | 51 | 90 | 7 | 1 |
| | 17 | 51 | 180 | 1 | 1 |
| | 18 | 51 | 180 | 3 | 1 |
| | 19 | 51 | 180 | 5 | 1 |
| | 20 | 51 | 180 | 7 | 1 |
| Half-circle | 18 | 29 | 90 | 0.55 | 0.55 |
| | 19 | 31 | 90 | 0.6 | 0.6 |
| | 20 | 33 | 90 | 0.65 | 0.65 |
| | 21 | 35 | 90 | 0.7 | 0.7 |
| | 22 | 39 | 90 | 0.75 | 0.75 |
| | 23 | 41 | 90 | 0.8 | 0.8 |
| | 24 | 43 | 90 | 0.85 | 0.85 |
| | 25 | 47 | 90 | 0.9 | 0.9 |
| | 26 | 49 | 90 | 0.95 | 0.95 |
| | 27 | 51 | 90 | 1 | 1 |

| Table 3.3 Experimental setup for COMSOL models investigating multiple rows of minipiles | | | | |
|---|---|---|---|---|
| Experiment Set | Case Number | Number of Minipiles n | Geometry | minipile layer setup (x/D) |
| Multirow | 28 | 91 | triangular | 0.75, 1 |
| | 29 | 102 | triangular | 0.75, 1.25 |
| | 30 | 115 | triangular | 1, 1.25 |
| | 31 | 154 | triangular | 0.75, 1, 1.25 |
| | 32 | 91 | half-circle | 0.75, 1 |
| | 33 | 102 | half-circle | 0.75, 1.25 |
| | 34 | 115 | half-circle | 1, 1.25 |
| | 35 | 154 | half-circle | 0.75, 1, 1.25 |

| Table 3.4 Experimental setups for sacrificial pile COMSOL models. | | | | | |
|---|---|---|---|---|---|
| Experiment Set | Case Number | Number of Piles n | Wedge Angle ° | x Distance (x/D) | y Distance (y/D) |
| Sacrificial Pile | 36 | 0 | - | 0 | 0 |
| | 37 | 1 | - | 2 | 0 |
| | 38 | 1 | - | 4 | 0 |
| | 39 | 1 | - | 6 | 0 |
| | 40 | 1 | - | 8 | 0 |

## 3.4 Data Analysis

The effect of different mini-pile configurations on the scour potential is evaluated based on the maximum normalized shear stress, $\tau'$, and weighted critical zone area, $A_{wcz}$, following Tao (2013) and Li (2018). How these parameters change in the 2D COMSOL models is taken as an indicator of how scour behaves in more complex scenarios (3D models or experimental).

Normalized shear stress is a unitless parameter that describes the shear stress in the model when normalized to the critical shear stress of the bed material. For a 2D system I can calculate the normalized shear stress as a function of the input flow velocity and the critical velocity:

$$\tau' = \frac{\tau}{\tau_c} = \frac{\rho_w v^2}{\rho_w v_c^2} = \frac{v^2}{v_c^2} \tag{3.2}$$

The maximum normalized shear stress is then given by COMSOL as the highest value in the area of interest. The critical zone area, $A_{cz}$, within the model is defined as the total area nearby the bridge pier that has shear stresses exceeding $\tau_c$. I modify the critical zone area by weighting each area with the corresponding normalized shear stress:

$$A_{wcz} = \int \tau' A_{cz} \tag{3.3}$$

For $A_{wcz}$ the integral is limited to within one topwidth, $T_w$, of the scour hole, which is approximately 4 bridge pier diameters (Arneson 2012). With the models complete and data analysis done I can look to the results.

# Chapter 4

# RESULTS

## 4.1 Introduction

Various geometries of sacrificial minipiles have been modeled in a 2D plane to explore how changing hydrodynamics modified local scour. To this end, I look to both the weighted critical zone area, $A_{wcz}$, and the maximum normalized shear stress, $\tau'$, within one scour topwidth of the pile I attempt to protect. One scour topwidth in my model corresponds to 4 times the main pile diameter.

Initial simulations compared circles to semi-circles with varying arc-length, and diamonds to triangles which showed that for unidirectional flow, the minipiles in the downstream area have limited effect on the velocity patterns. Subsequent more in-depth analysis for which the results are presented in this paper focused on triangles and half-circles only (Table 4.1)

## 4.2 Triangular Geometries

Results for the triangular geometries are tabulated in Table 4.1. Figure 4.1 and 4.2 show the graphical results comparing τ' and $A_{wcz}$ as functions of the Normalized

Distance from the center of the main bridge pier. The results demonstrate that all triangular configurations reduce the maximum critical shear, except for the 90° case that shows an increase in the maximum normalized shear within the top-width at close distance from the main pile.  which decreases when the system is moved further upstream of the main pile. The 90° minipile system also shows a similar trend for the weighted critical zone area, the value decreases as the system is placed further away from the central pile.

| Table 4.1 Result Parameters for Triangular and Half-circle Models | | | | | | | | |
|---|---|---|---|---|---|---|---|---|
| Experiment Set | Case # | # of Minipiles n | Wedge Angle ° | x Distance (x/D) | y Distance (y/D) | $A_{cz}$ m² | $A_{wcz}$ m² | $\tau'$ |
| Triangular | 1 | 39 | 90 | 0.75 | 0.75 | 0.0412 | 0.0479 | 1.6935 |
| | 2 | 41 | 90 | 0.8 | 0.8 | 0.0406 | 0.0470 | 1.6717 |
| | 3 | 43 | 90 | 0.85 | 0.85 | 0.0404 | 0.0467 | 1.6800 |
| | 4 | 47 | 90 | 0.9 | 0.9 | 0.0399 | 0.0460 | 1.6669 |
| | 5 | 49 | 90 | 0.95 | 0.95 | 0.0401 | 0.0461 | 1.6807 |
| | 6 | 51 | 90 | 1 | 1 | 0.0396 | 0.0454 | 1.6570 |
| | 7 | 63 | 90 | 1.25 | 1.25 | 0.0373 | 0.0418 | 1.6515 |
| | 8 | 33 | 53.6 | 1.29 | 0.65 | 0.0416 | 0.0476 | 1.3167 |
| | 9 | 51 | 53.6 | 1.98 | 1 | 0.0404 | 0.0456 | 1.5013 |
| | 10 | 63 | 53.6 | 2.45 | 1.25 | 0.0393 | 0.0435 | 1.5113 |
| | 11 | 29 | 20 | 3.12 | 0.55 | 0.0410 | 0.0461 | 1.3927 |
| | 12 | 51 | 20 | 5.67 | 1 | 0.0406 | 0.0449 | 1.2243 |
| | 13 | 63 | 20 | 7.03 | 1.25 | 0.0381 | 0.0415 | 1.2438 |
| | 14 | 51 | 90 | 3 | 1 | 0.0331 | 0.0349 | 1.3447 |
| | 15 | 51 | 90 | 5 | 1 | 0.0321 | 0.0334 | 1.4026 |
| | 16 | 51 | 90 | 7 | 1 | 0.0338 | 0.0354 | 1.3734 |
| | 17 | 51 | 180 | 1 | 1 | 0.0403 | 0.0450 | 1.3441 |
| | 18 | 51 | 180 | 3 | 1 | 0.0353 | 0.0375 | 1.3762 |
| | 19 | 51 | 180 | 5 | 1 | 0.0337 | 0.0355 | 1.4943 |
| | 20 | 51 | 180 | 7 | 1 | 0.0333 | 0.0350 | 1.5259 |
| Half-circle | 21 | 29 | 90 | 0.55 | 0.55 | 0.0313 | 0.0381 | 1.3569 |
| | 22 | 31 | 90 | 0.6 | 0.6 | 0.0313 | 0.0381 | 1.4184 |
| | 23 | 33 | 90 | 0.65 | 0.65 | 0.0309 | 0.0376 | 1.4309 |
| | 24 | 35 | 90 | 0.7 | 0.7 | 0.0310 | 0.0377 | 1.4268 |
| | 25 | 39 | 90 | 0.75 | 0.75 | 0.0312 | 0.0376 | 1.4503 |
| | 26 | 41 | 90 | 0.8 | 0.8 | 0.0315 | 0.0380 | 1.4504 |
| | 27 | 43 | 90 | 0.85 | 0.85 | 0.0313 | 0.0375 | 1.4563 |
| | 28 | 47 | 90 | 0.9 | 0.9 | 0.0310 | 0.0369 | 1.4683 |
| | 29 | 49 | 90 | 0.95 | 0.95 | 0.0312 | 0.0371 | 1.4729 |
| | 30 | 51 | 90 | 1 | 1 | 0.0313 | 0.0373 | 1.4822 |

s

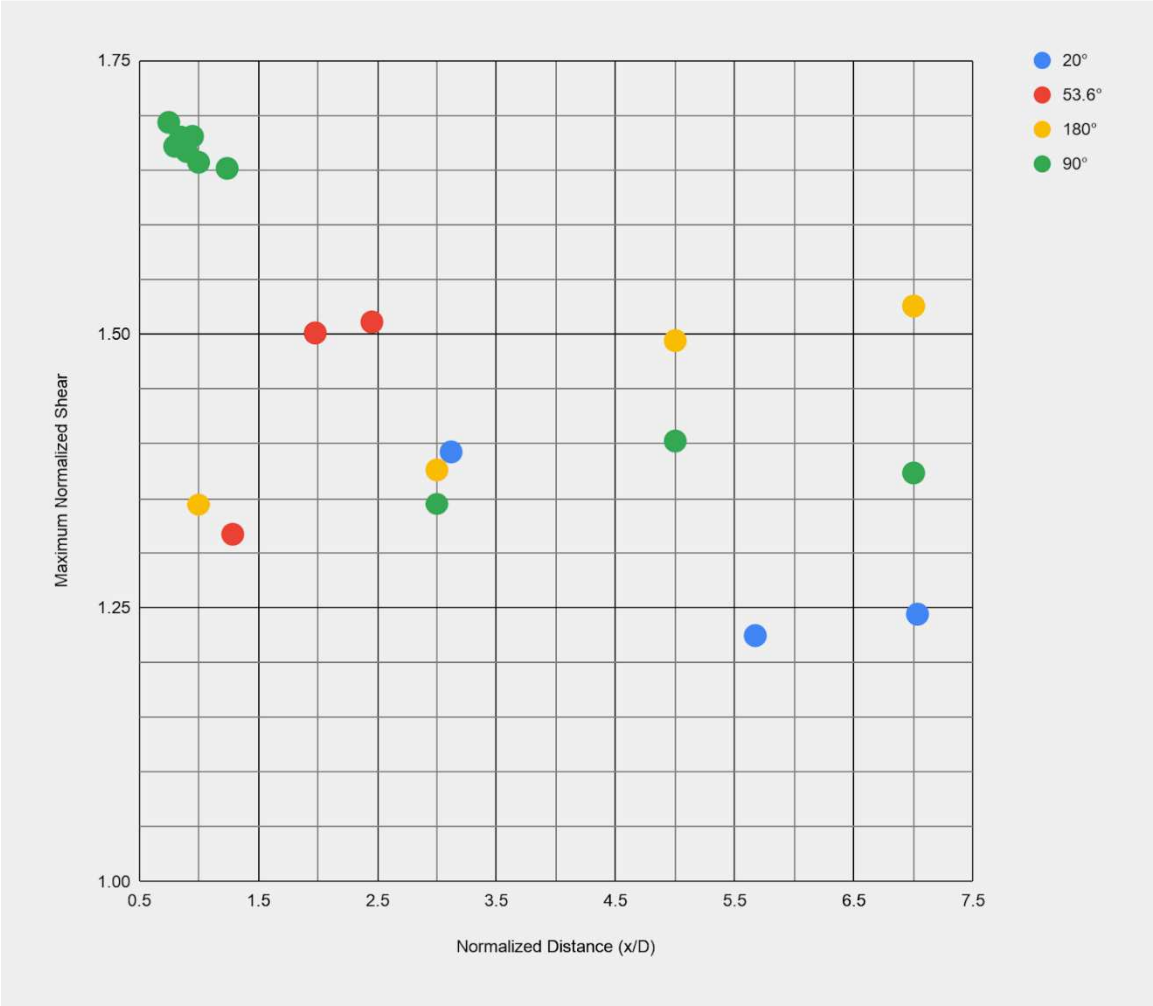


**Figure 4.1** Maximum Normalized shear for the triangular minipile geometries, with varying distance between the front minipile and the major pile.

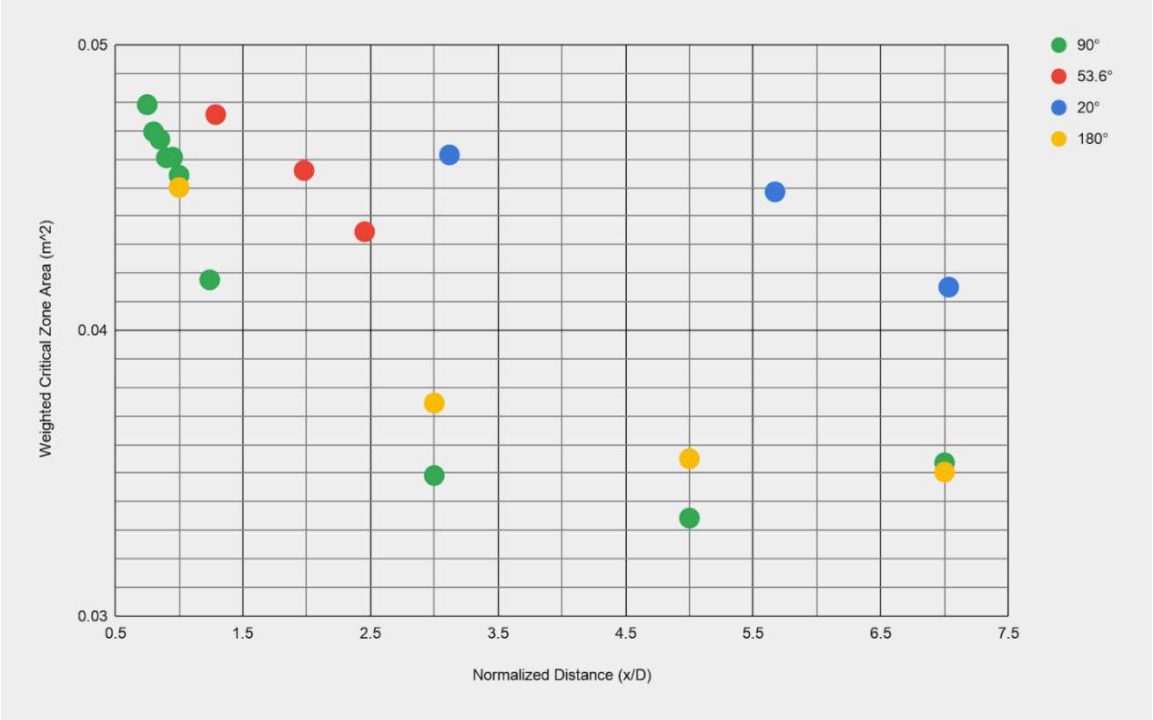


**Figure 4.2** Weighted Critical Zone Area for the triangular minipile geometries with varying distances between the front minipile and the major pile.

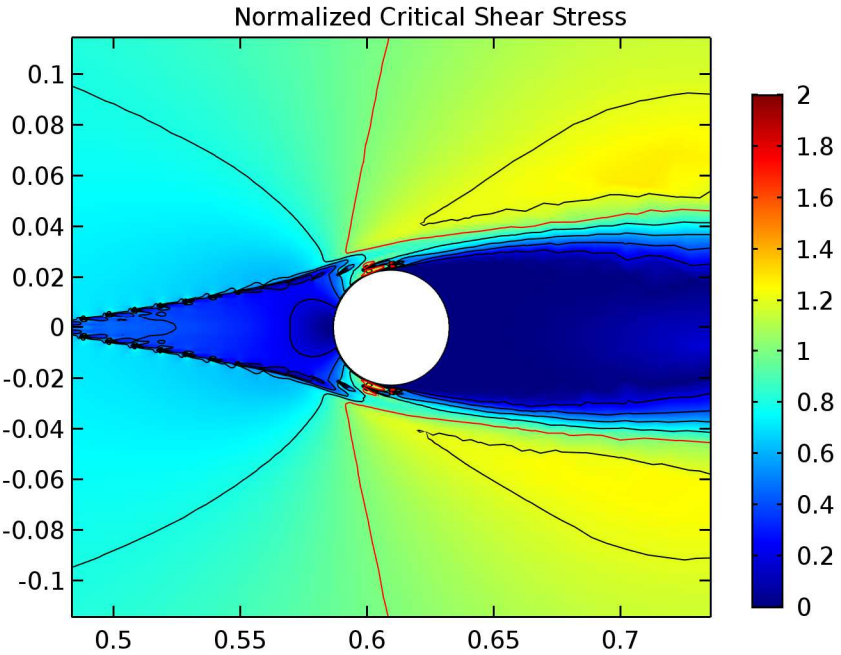


**Figure 4.3** Normalized Critical Shear Stress distribution within ½ Tw of the central monopile for Case # 11.

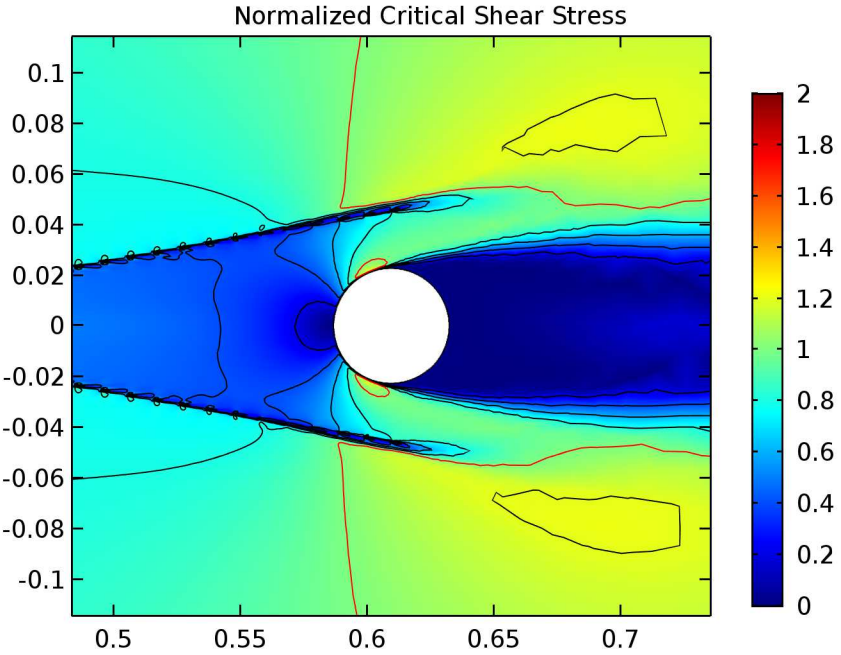


**Figure 4.4** Normalized Critical Shear Stress distribution within ½ Tw of the central monopile for Case # 12.

4.3 Half-circle Geometry

Parameter results for the half-circle geometries (case #'s 21-30) are tabulated in Table 4.1. Comparisons in $A_{cz}$, $A_{wcz}$, and $\tau'_{max}$ as functions of the normalized center to center distance from the main bridge pier are found in Figures 4.3 and 4.4. The half-circle geometries were built at different center-to-center distances from the main pile. The models maintain fairly consistent $A_{cz}$ and $A_{wcz}$ across increasing distance from the main pile while the maximum normalized shear increases as the minipile system is moved to further distances from the major pile.

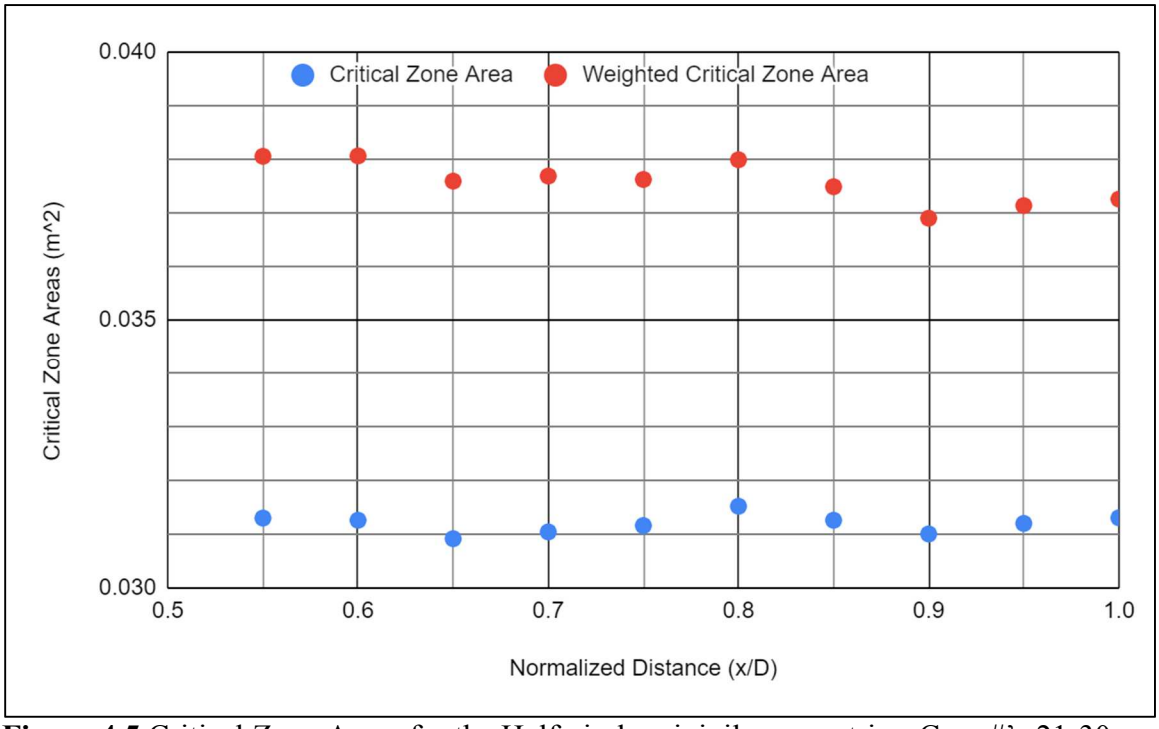


**Figure 4.5** Critical Zone Areas for the Half-circle minipile geometries, Case #'s 21-30.

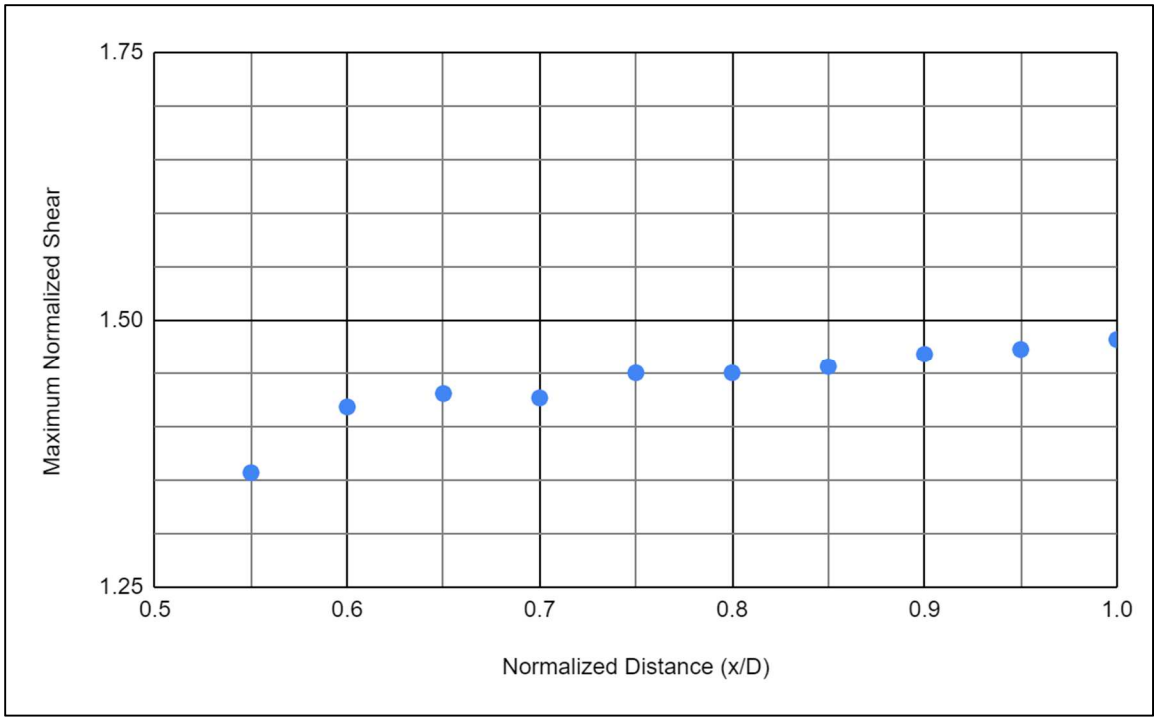


**Figure 4.6** Maximum Normalized Shear for the circular minipile geometries.

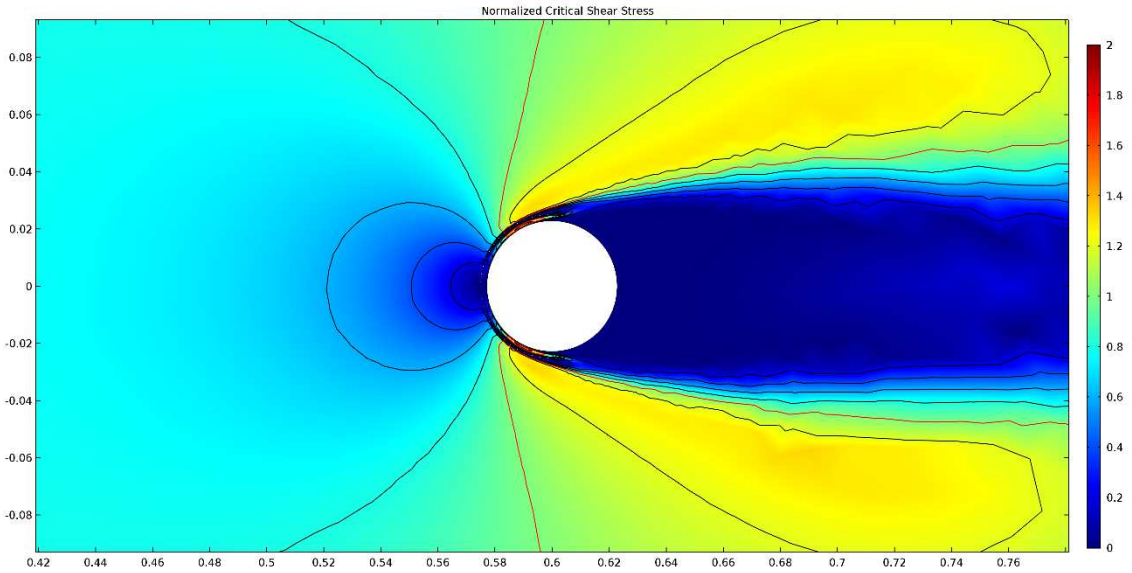


**Figure 4.7** Normalized Critical Shear Stress for Case #21.

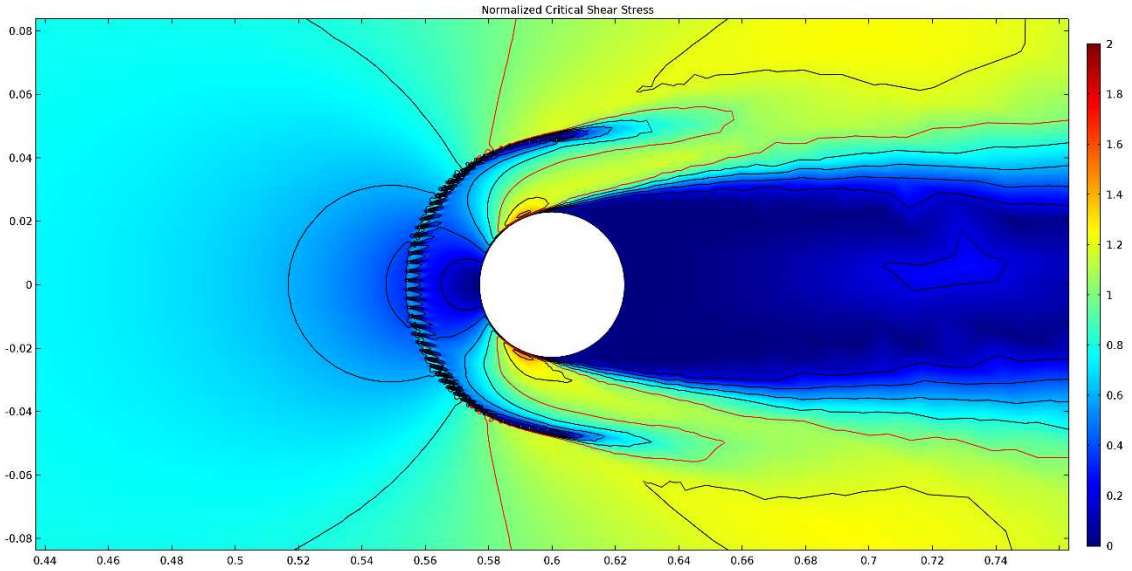


**Figure 4.8** Normalized Critical Shear Stress for Case #30.

## 4.4 Multirow Systems

Model results for multi-row systems with triangular and circular geometries are tabulated in Table 4.2. Figures 4.9 and 4.10 compare the triangular multi-row systems to similar triangular setups in earlier model runs.

| Table 4.2 Experimental setup for COMSOL models investigating multiple rows of minipiles | | | | | | | |
|---|---|---|---|---|---|---|---|
| Experiment Set | Case # | # of minipiles n | Geometry | Minipile layer setup (x/D) | $A_{cz}$ m² | $A_{wcz}$ m² | $\tau'$ |
| Multirow | 31 | 91 | triangular | 0.75, 1 | 0.0404 | 0.0476 | 1.7092 |
| | 32 | 102 | triangular | 0.75, 1.25 | 0.0390 | 0.0459 | 1.6902 |
| | 33 | 115 | triangular | 1, 1.25 | 0.0390 | 0.0458 | 1.7190 |
| | 34 | 154 | triangular | 0.75, 1, 1.25 | 0.0399 | 0.0481 | 1.7569 |
| | 35 | 91 | half-circle | 0.75, 1 | 0.0414 | 0.0508 | 1.3622 |
| | 36 | 102 | half-circle | 0.75, 1.25 | 0.0422 | 0.0512 | 1.3622 |
| | 37 | 115 | half-circle | 1, 1.25 | 0.0404 | 0.0486 | 1.3661 |
| | 38 | 154 | half-circle | 0.75, 1, 1.25 | 0.0410 | 0.0510 | 1.3544 |

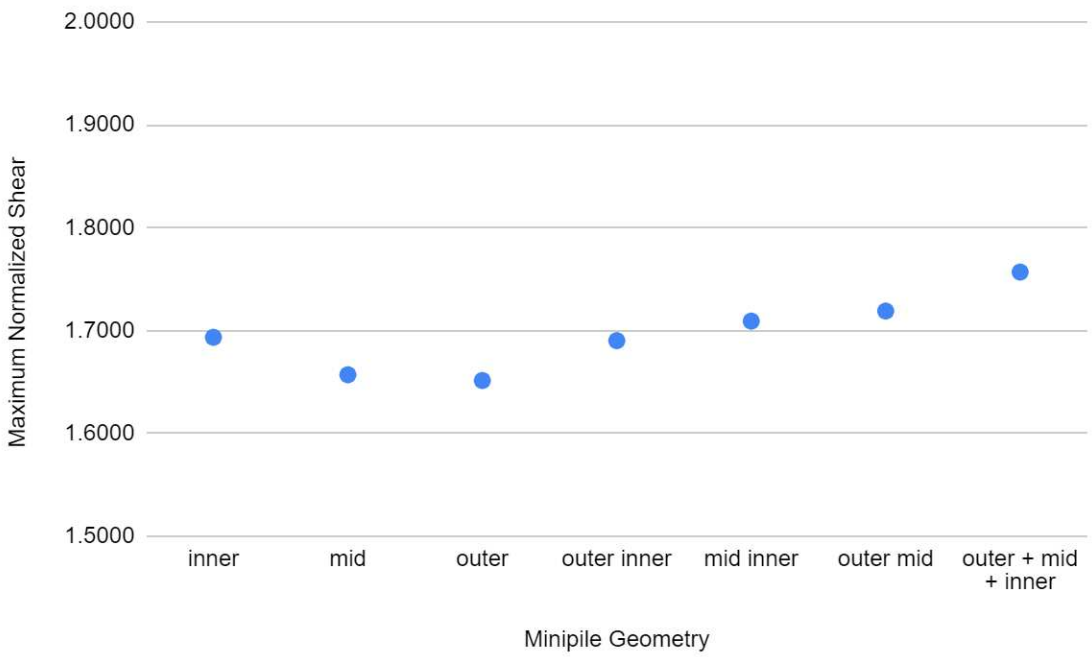


**Figure 4.9** Maximum Normalized Shear for the multirow experiment case #'s 31-34 compared to case #'s 1, 6, and 7.

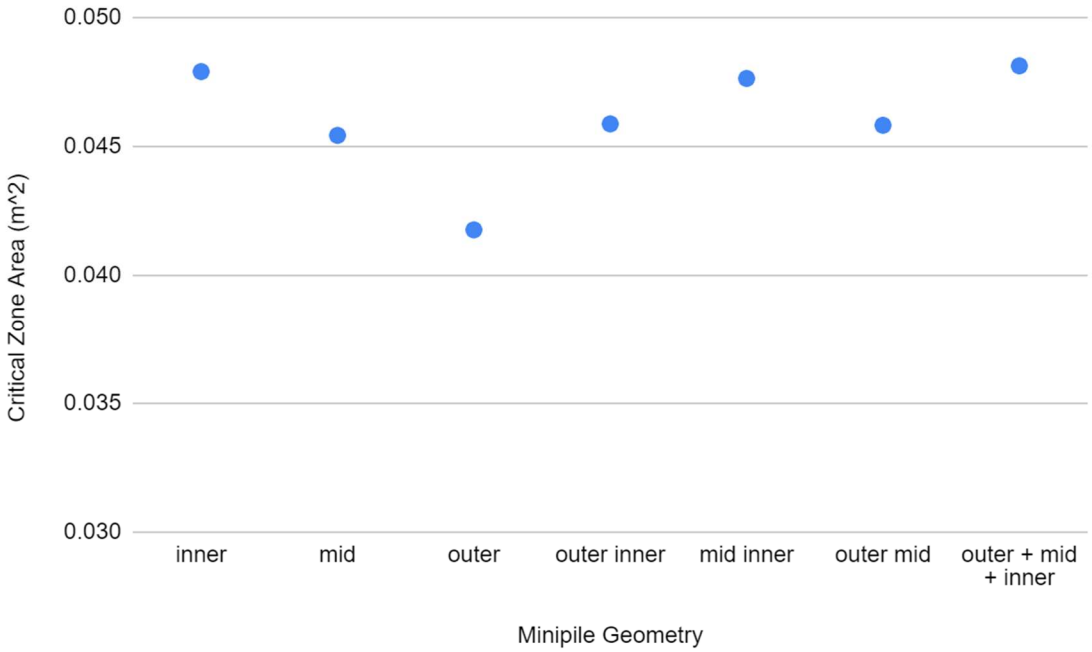


**Figure 4.10** Weighted Critical Zone Areas for multirow case #'s 31-34 compared to case #'s 1, 6, and 7.

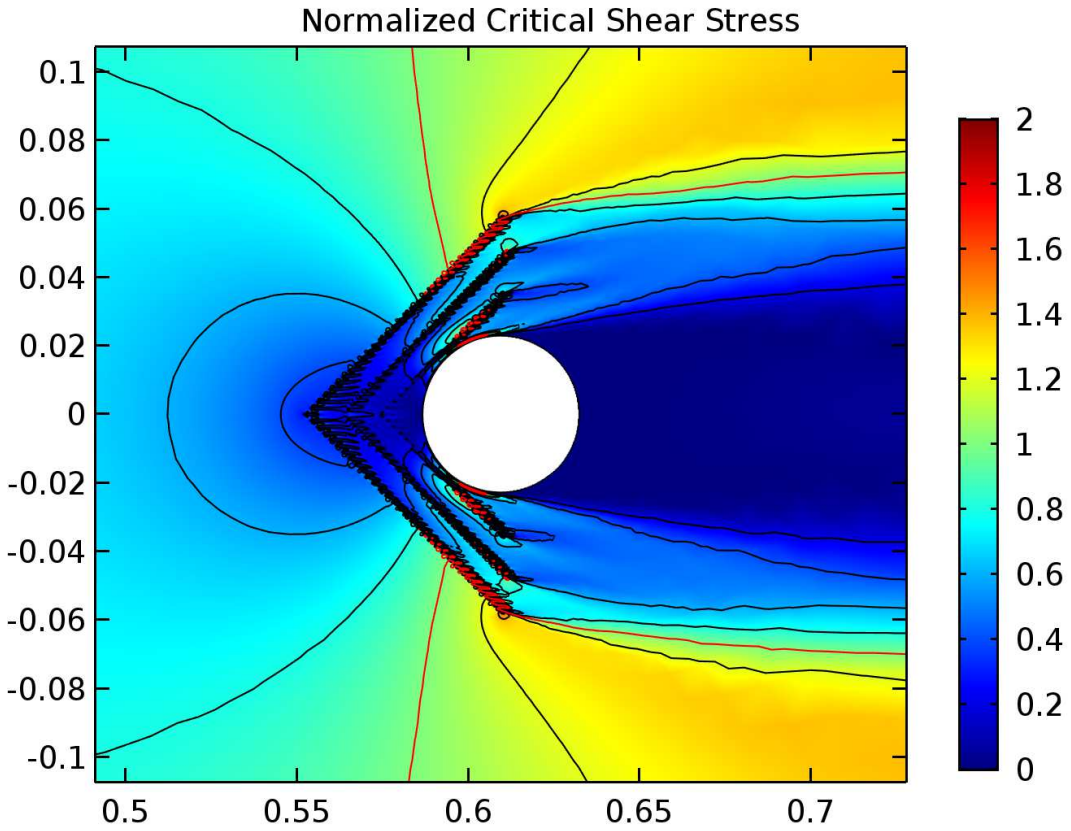


**Figure 4.11** Normalized critical shear stress for multirow case # 34, the three layer triangular configuration.

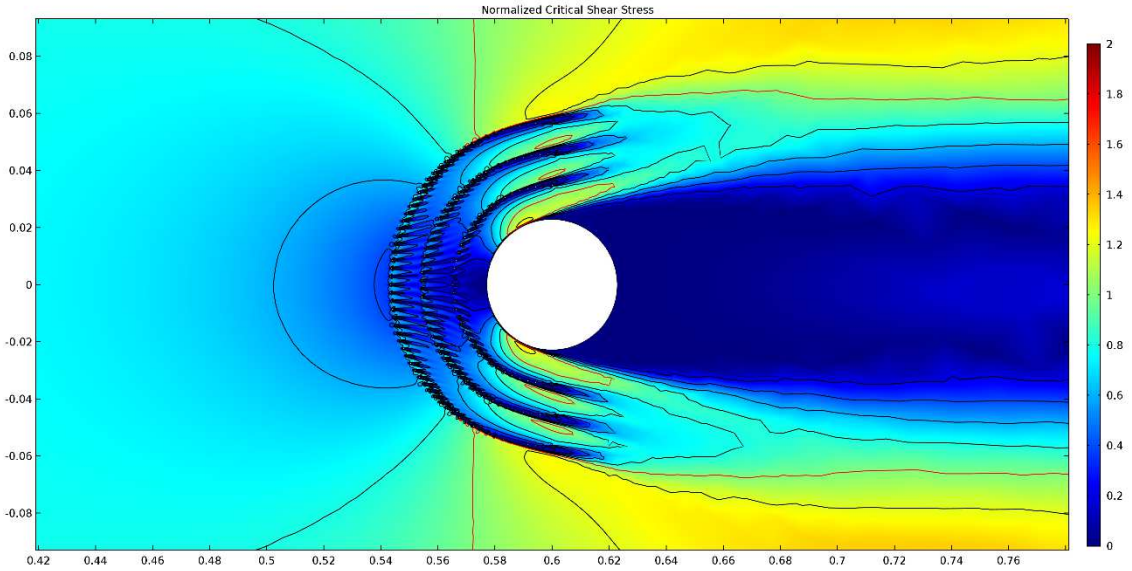


**Figure 4.12** Normalized Critical Shear for multirow case # 38, the three layer half-circle configuration.

## 4.5 Simple Sacrificial Pile

A simple sacrificial pile system was also modeled where a sacrificial pile of the same diameter as the bridge pier was placed at various distances upstream. Values for Maximum Normalized Shear and for Weighted Critical Zone Areas can be seen in Figures 3.5 and 3.6.

| Table 4.3 Experimental setups for sacrificial pile COMSOL models. | | | | | | | | |
|---|---|---|---|---|---|---|---|---|
| Experiment Set | Case # | # of Piles n | Wedge Angle ° | x Distance (x/D) | y Distance (y/D) | $A_{cz}$ m² | $A_{wcz}$ m² | $\tau'_{max}$ |
| Sacrificial Pile | 39 | 0 | - | 0 | 0 | 0.0202 | 0.0219 | 1.6078 |
| | 40 | 1 | - | 2 | 0 | 0.0258 | 0.0275 | 1.6158 |
| | 41 | 1 | - | 4 | 0 | 0.0584 | 0.0616 | 1.5105 |
| | 42 | 1 | - | 6 | 0 | 0.0618 | 0.0636 | 1.5609 |
| | 43 | 1 | - | 8 | 0 | 0.0378 | 0.0397 | 1.6033 |

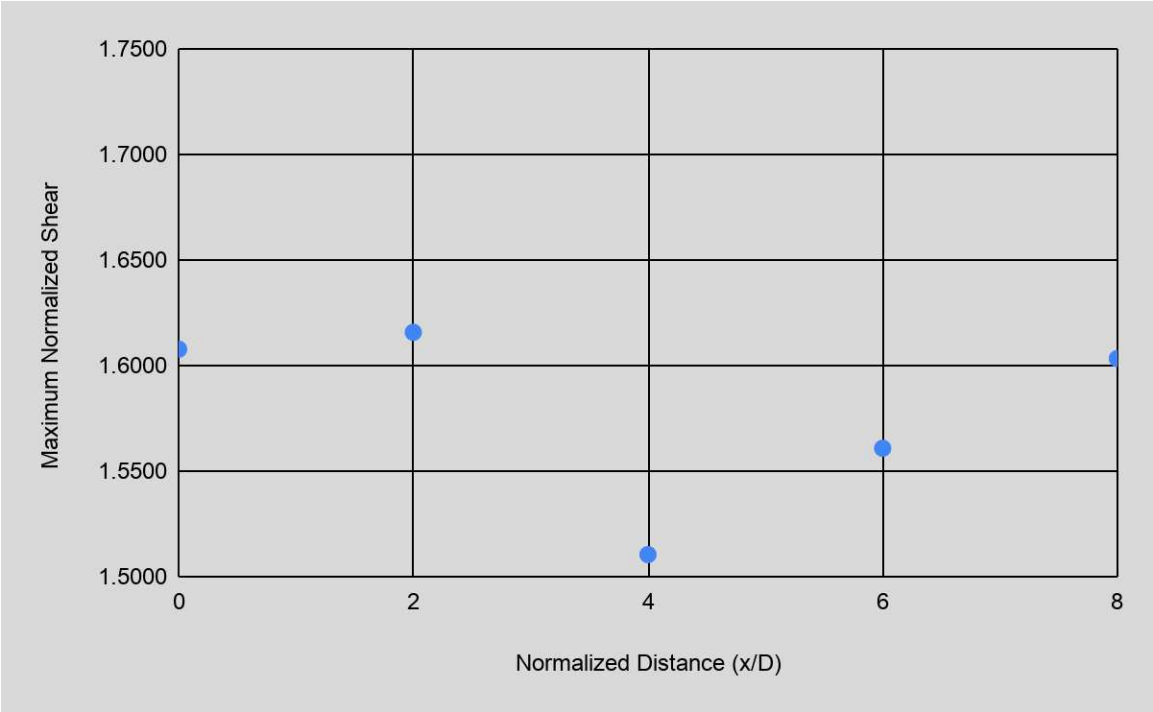


**Figure 4.13** Maximum Normalized Shear for the Sacrificial Pile setups.

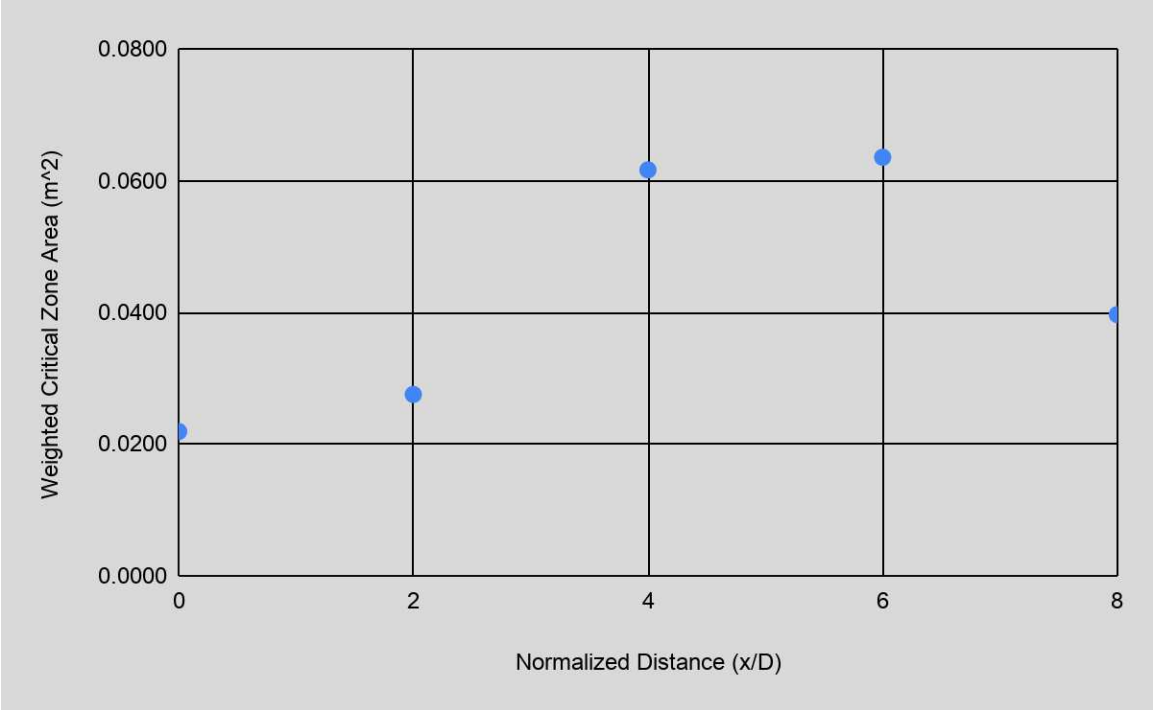


**Figure 4.14** Weighted Critical Zone Areas for the Sacrificial Pile setups.

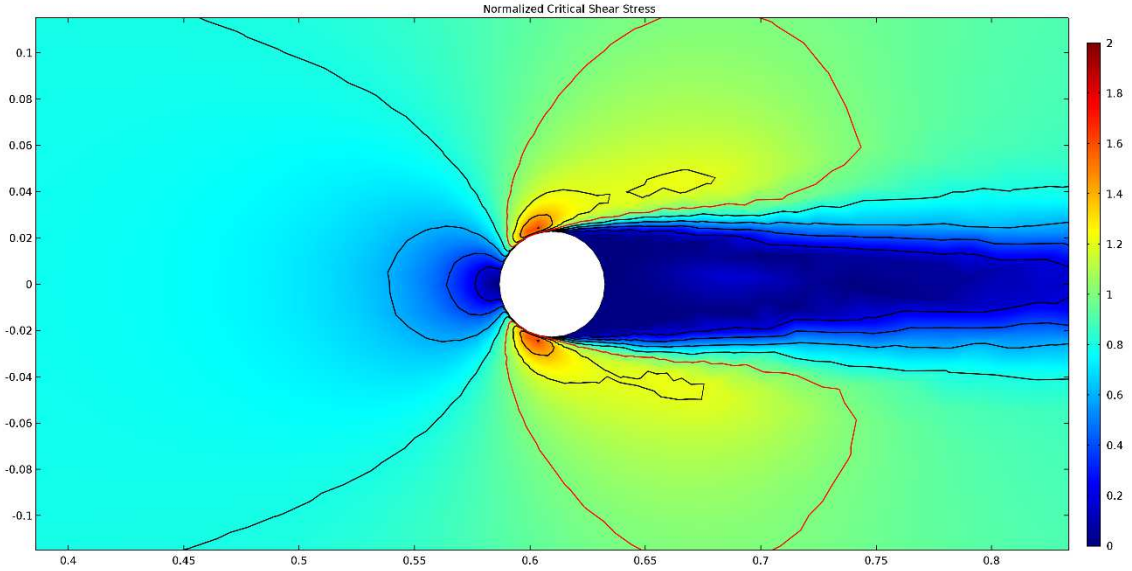


**Figure 4.15** Case # 39, the control case for

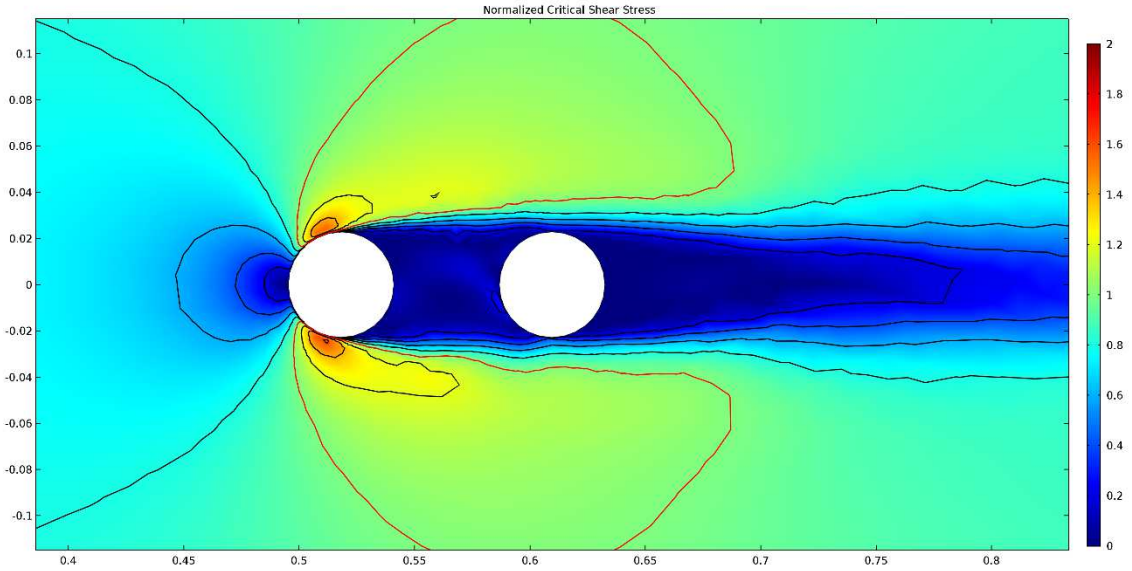


**Figure 4.16** Case # 40

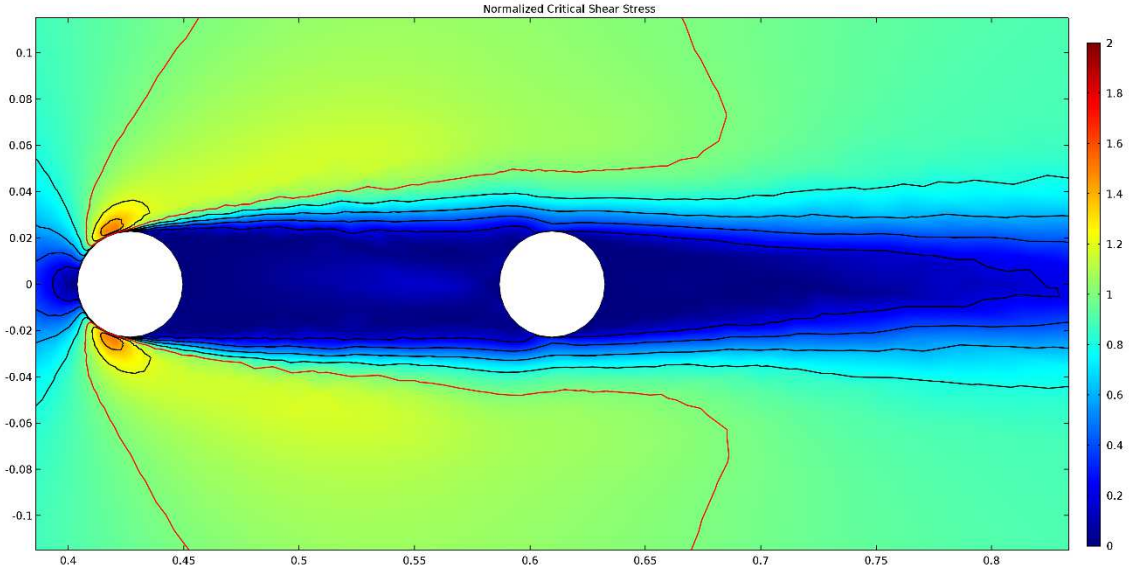


**Figure 4.17** Case #41

# Chapter 5

# DISCUSSION

The modeled systems have complex relationships between the maximum normalized shear and the weighted critical areas. An optimal mini-pile setup would reduce both $\tau'_{max}$ and $A_{wcz}$ within the COMSOL models and correlate with reduced scour around a similar setup in the real world. At worst, the models should produce comparable results to a sacrificial pile system, i.e. provide a baseline of mitigation against scour. Further, if the mini-pile systems can perform at a higher level than the sacrificial pile system for less material cost the mangrove inspired systems merit further experiments in both 3D CFD and in experimental flumes.

## 5.1 Comparisons to the Standard

First of all, how do the mini-pile systems compare to the just leaving a single bridge pier (Case #39) in the same flow? In all cases where the farthest mini-pile is placed more than 2 diameters upstream of the central pile, $\tau'_{max}$ is reduced. However, no experiment reduces $A_{wcz}$ or $A_{cz}$ below the initial values for Case #39 (without any scour mitigation measure). This is due to flow being forced around the bridge pier to be faster due to water contraction effect due to the added obstacles to flow. This will change the

ultimate scour characteristics in the river system, but it is unclear if this will also negatively affect the local scour around the bridge pier.

Secondly, we should also ask how the mini-pile systems compare to the larger sacrificial pile simulations (Case #'s 41-43). The $\tau'_{max}$ is not notably different for the sacrificial pile compared to the base case #39. However, as demonstrated in the field the sacrificial pile reduces the shear velocity and mitigates scour around a bridge pier. As the sacrificial pile is moved upstream the maximum normalized shear decreases – possibly an artifact of the model dimensions (Figure 4.13). Several mini-pile configurations tend to outperform the sacrificial pile experiments. Notably the acute triangular configurations (Case #'s 8-20) and the half-circle configurations (Case #'s 21-30 & 35-38) perform as well as or better than the best sacrificial pile configuration (Case # 41) in terms of $\tau'_{max}$. For $A_{wcz}$, the best sacrificial pile configuration (Case #40) outperforms all minipile cases. However, as a point in their favor, the mini-pile cases all have lower $A_{wcz}$ than the other sacrificial pile configurations.

To estimate the material costs the volume of the sacrificial pile is compared to the cumulative volume of mini-piles as shown in Table 5.1. In this thought experiment, the total area of the mini-piles in a Case #'s experiment is taken to be analogous to material cost. To further simplify, the cost of the mini-pile and sacrificial pile materials are equalized. Then the 'cost' of the system can be compared to the performance parameters $A_{wcz}$ and $\tau'_{max}$.

| Table 5.1 Estimation of Material Cost and Performance | | | | | | | |
|---|---|---|---|---|---|---|---|
| Case # | $A_{cz}$ m² | $A_{wcz}$ m² | $\tau'_{max}$ | Normalized Area of pile group $A_{pilegroup}/A_{sacpile}$ | Number mini-piles | $A_{wcz}$ $/A_{norm}$ | $\tau'_{max}$ $/A_{norm}$ |
| 9 | 0.0404 | 0.0456 | 1.5013 | 0.0051 | 51 | 0.1118 | 0.0034 |
| 14 | 0.0331 | 0.0349 | 1.3447 | 0.0051 | 51 | 0.1461 | 0.0038 |
| 22 | 0.0313 | 0.0381 | 1.4184 | 0.0031 | 31 | 0.0814 | 0.0022 |
| 41 | 0.0584 | 0.0616 | 1.5105 | 1 | - | 16.2217 | 0.6621 |
| 42 | 0.0618 | 0.0636 | 1.5609 | 1 | - | 15.7330 | 0.6407 |

Clearly the mini-pile systems require a significantly lower amount of material to be installed and therefore may be economically favorable. However a full cost analysis should include material types, installation of mini-pile systems, and maintenance costs.

## 5.2 Comparisons between Minipile Systems

Within the triangular minipile experiments there are clear winners. The best performers have at least one thing in common across all geometries: placement further upstream of the bridge pier. Further, depending on which parameter between $A_{wcz}$ and $\tau'_{max}$ is considered to be a better indicator of scour, you may value the acute triangular set (Case #'s 8-13) ahead of the migrating triangular set (Case #'s 14-20), corresponding to Melville et al (1999). Within the half-circle set, all perform well and again depending on the relative value of $A_{wcz}$ and $\tau'_{max}$, they can be ranked differently.

## 5.3 Future Investigations

A big question from this work to carry forward is primarily how good the parameters are that I measure for determining scour in a real system. In this study cases were compared following the approach suggested by Tao & Li (20xx), using $\tau'_{max}$ within 4 diameters around the main pile and $A_{wcz}$. This method has been empirically validated for more simple systems (e.g. single bridge piers of different diameters under different flow conditions, see HEC-18) and were used to look at differently shaped piers (Li 2018) but not necessarily for pier groups, much less a single larger pier surrounded by a complex configuration of smaller mini-piles.

The actual scour is affected by the flow in vertical directions, e.g. through horseshoe vortices. Vertical flow cannot be simulated in my 2D models, however zones with low horizontal flow velocity, steep velocity gradients or high turbulence may correlate to zones with increased vertical velocity (eg. high $A_{wcz}$). More in depth analysis of the 2D simulations should be performed or 3D CFD simulations and flume experiments should be run to couple shear stress to scour depth and location to ultimately test this question and identify how useful my parameters to estimate scour actually are. A suggestion then is to model a variety of modified $A_{wcz}$ and $\tau'_{max}$ parameters to determine which most accurately and precisely describe scour across 2D models, 3D models, flume experiments, and field trials.

# Chapter 6

# CONCLUSIONS

Bridge scour at piers is a major problem for designing new and maintaining existing infrastructure. The current methods require their own upkeep and there may be better ways to mitigate scour. In this study I looked to the mangrove forests of coastal environments for inspiration and have developed a 2D numerical model to test the efficacy of placing a mangrove-root inspired system of mini-piles to mitigate scour around a submerged pile foundation in a confined singular flow direction (river case). Experimental flume dimensions were used to create a model to explore these scour parameters and may not directly applicable to field scale. This study focused on how the configuration of the mini-piles affects the hydrodynamics surrounding a submerged foundation.

The simulations demonstrated that adding a mangrove inspired configuration of mini-pile in front of bridge piers changes scour parameters. Compared to larger sacrificial piles, the mini-pile systems reduce $A_{wcz}$ and $\tau'_{max}$ by similar (or even better) amounts, which could result in an overall favorable in terms of the volume of material added. The simulations demonstrated that it is more benefit to place minipile systems upstream of the main bridge pier in an acute triangular as their own 'mangrove forest'. The value of $A_{wcz}$ and $\tau'_{max}$ for complex 2D models of scour is unclear and 3D CFD simulations and physical experiments need to be performed to verify the methodology and conclusions.

This is in part due to the limiting nature of my simulations being conducted as 2D slices of the bridge-river system as well as being unvalidated. Therefore, future work should be conducted to test ‘mangrove forest’ mini-pile systems in 3D space, in flume experiments, and in field trials to figure out which parameters best match up across experiments to predict scour locations or scour depth.

# REFERENCES


Adame, M.F., Neil, D., Wright, S.F., Lovelock, C.E. (2010). Sedimentation within and among mangrove forests along a gradient of geomorphological settings. *Estuarine, Coastal, and Shelf Science*, Vol. 86, pp. 21-30.

Andrade, R.A., Sanders, C.J., Boaventura, G., Patchineelam, S.R. (2012) Pyritization of trace metals in mangrove sediments. *Environmental Earth Science*, Vol. 67, pp. 1757-1762.

Arneson, L.A., Zevenbergen, L.W., Lagasse, P.F., Clopper, P.E. (2012). Evaluating Scour at Bridges. *Hydraulic Engineering Circular 18, Fifth Edition*, FHWA HIF-12-003, Federal Highway Administration, U.S. Department of Transportation, Washington D.C.

Chen, Z., Ortiz, A., Zong, L., Nepf, H. (2012). The wake structure behind a porous obstruction and its implications for deposition near a finite patch of emergent vegetation. *Water Resources Research*, Vol. 48.

Chiew, Y. M. (1995). Mechanics of Riprap Failure at Bridge Piers. *Journal of Hydraulic Engineering*, ASCE, Vol. 121, No. 9, pp. 635-643.

Chiew, Y. M. (2002). Failure mechanisms of riprap layer around bridge piers. *First International Conference on Scour of Foundations,* Texas, USA, pp. 70–91.

Cook, W. (2014). Bridge Failure Rates, Consequences, and Predictive Trends. Ph.D. dissertation at Utah State University.

DNV (2010). Design of Offshore Wind Turbine Structures. DNV-OS-J101, Det Norske Veritas.

Flint, M.M, Fringer, O., Billington, S.L., Freyberg, D., Diffenbaugh, N.S. (2017). Historical Analysis of Hydraulic Bridge Collapses in the Continental U.S. *Journal of Infrastructure Systems*, Vol. 23.

Guannel, G., Arkema, K., Ruggiero, P., Verutes, G. (2016). The Power of Three: Coral Reefs, Seagrasses and Mangroves protect Coastal Regions and Increase Their Resilience. *PLoS ONE*. ("doi:19,1371/journal.pone.0158094)

Hunt, B.E. (2009). Monitoring scour critical bridges: A synthesis of highway practice. NCHRP Synthesis 396, Transportation Research Board.

Kazemi, A., Van de Riet, K., Curet, O.M. (2017). Hydrodynamics of mangrove-type root models: the effect of porosity, spacing ratio, and flexibility. *Bioinspiration and Biomimetics*, Vol. 12.

Kazemi, A., Van de Riet, K., Curet, O.M.(2018). Drag coefficient and flow structure downstream of mangrove root-type models through PIV and direct force measurements. *Physical Review Fluids*, Vol. 3,

Khosronejad, A., Kang, S., and Sotiropoulos, F.(2012). Experimental and computational investigation of local scour around bridge piers. *Advances in Water Resources*, Vol. 37, pp. 73-85.

Lagasse, P.F., Clopper, P.E., Pagan-Ortiz, J.E., Zevenbergen, L.W., Arneson, L.A., Schall, J.D., Girard, L.G. (2009). Bridge Scour and Stream Instability Countermeasures: Experience, Selection, and Design Guidance-Volume 1. *Hydraulic Engineering Circular 23, Third Edition*, FHWA NHI-09-111, U.S. Department of Transportation, Washington D.C.

Li (2018). Pier Streamlining As a Bridge local Scour Countermeasure and the Underlying Scour Mechanism. Ph.D. dissertation at the University of Akron.

Melville, B.W., Sutherland, A.J. (1988). Design Method for Local Scour at Bridge Piers. *Journal of Hydraulic Engineering*, Vol. 114, pp. 1210-1226.

Melville, B.W., and Hadfield, A.C. (1999). Use of Sacrificial Piles as Pier Scour Countermeasures. *Journal of Hydraulic Engineering*, Vol. 125, pp. 1221-1224.

Mendoza, U.M.N. (2007). Dynamics of phosphorus and sulphur in a mangrove forest in Bragança, North Brazil. Ph.D. dissertation at Universität Bremen.

Molinas, A. (2001). Effects of Gradation and Cohesion on Bridge Scour: Synthesis Report, Report No. FHWA-RD-99-189, Federal Highway Administration, Washington, DC.

Mueller, D.S. (1996). Local Scour at Bridge Piers in Nonuniform Sediment Under Dynamic Conditions. Ph.D. dissertation at Colorado State University.

Nazari-Sharabian, M., Nazari-Sharabian, A., Karakouzian, M., Karami, M. (2020). Sacrificial Piles as Scour Countermeasures in River Bridges A Numerical Study using *FLOW-3D*. *Civil Engineering Journal*, ASCE, Vol. 6, pp. 1091-1103.

Ola, A., Dodd, I.C., Quinton, J.N. (2015). Can we manipulate root system architecture to control soil erosion? *Soil*, Vol. 1, pp. 603-612.

Richardson, E.V. and Davis, S.R. (2001). Evaluating Scour at Bridges. *Hydraulic Engineering Circular No. 18, Fourth Edition*, Publication No. FHWA-NHI-01-001, Federal Highway Administration, Washington, DC.

Shen, H.W., Schneider, V.R., Karaki, S.S. (1966). Mechanics of Local Scour. U.S. Department of Commerce, National Bureau of Standards, Institute for Applied Technology, Washington, DC.

Sumer, B.M., Nielsen, A. (2013). Sinking failure of scour protection at wind turbine foundation. *Proceedings of the Institution of Civil Engineers – Energy*, Vol. 166, pp. 170-188.

Tao, J. (2013). Fusion of Numerical Modeling and Innovative Sensing to Advance Bridge Scour Research and Practice. Ph.D. dissertation at Case Western Reserve University.

Tomizcek, T., Wargula, A., Lomonaco, P., Goodwin, S., Cox, D., Kennedy, A., Lynett, P. (2020). Physical model investigation of mid-scale mangrove effects on flow hydrodynamics and pressures and loads in the built environment. *Coastal Engineering*, Vol. 162. (https://doi.org/10.1016/j.coastaleng.2020.103791)

Unger, J, and Hager W.H., (2007). Down-flow and horseshoe vortex characteristics of sediment embedded bridge piers. *Experimental Fluids*, Vol. 42, pp. 1-19.

U.S. Department of Transportation, Federal Highway Administration, (1988). Scour at Bridges. Technical Advisory T5140.20, updated by Technical Advisory T5140.23, October 28, 1991, "Evaluating Scour at Bridges," U.S. Department of Transportation, Washington, D.C.

Waldron, L.J. (1977). The Shear Resistance of Root-permeated Homogeneous and Stratified Soil. *Soil Science Society of America Journal*, Vol. 41, pp. 843-849.

# APPENDIX A

# CALCULATION OF MODEL PARAMETERS

Median grain size, $D_{50}$, was calculated from soil on hand in the experimental flume lab.

Table A.1 Sieve Data for experimental flume soil

| Sieve # | aperture size | Sieve Mass | Sieve & Soil Mass | Soil Mass | Cumulative Soil retained | Soil Passing | % Passing |
|---|---|---|---|---|---|---|---|
| | [mm] | [g] | [g] | [g] | [g] | [g] | [%] |
| 4 | 4.76 | 502 | 502 | 0 | 0 | 1015.5 | 100 |
| 8 | 2.36 | 476.3 | 482.1 | 5.8 | 5.8 | 1009.7 | 99.43 |
| 25 | 0.707 | 344.1 | 637 | 292.9 | 298.7 | 716.8 | 70.59 |
| 30 | 0.595 | 365.9 | 460 | 94.1 | 392.8 | 622.7 | 61.32 |
| 40 | 0.42 | 395.2 | 527.6 | 132.4 | 525.2 | 490.3 | 48.28 |
| 80 | 0.177 | 343.7 | 672.8 | 329.1 | 854.3 | 161.2 | 15.87 |
| 100 | 0.149 | 308.1 | 346.2 | 38.1 | 892.4 | 123.1 | 12.12 |
| 200 | 0.074 | 301 | 406.5 | 105.5 | 997.9 | 17.6 | 1.73 |
| Base ('fines') | | 362.1 | 379.7 | 17.6 | 1015.5 | 0 | 0 |

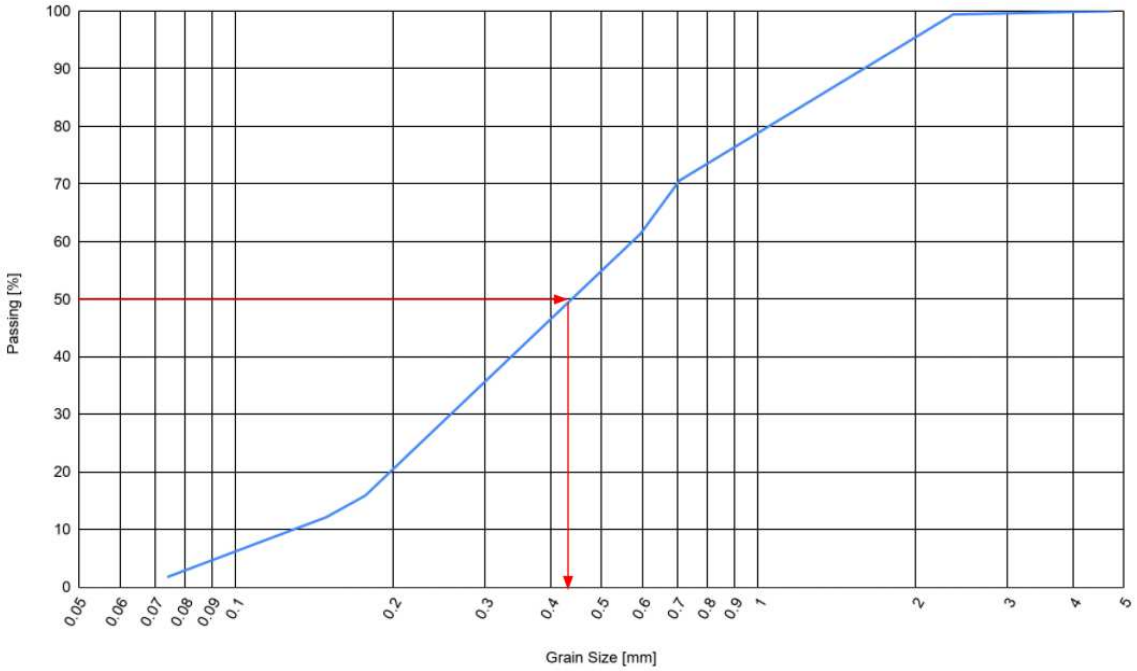


Figure A.1 Grain Size Distribution of Experimental Flume Soil and corresponding method of determining $D_{50} = 0.45$ mm.

Critical velocity, $v_c$, calculation was done with Eq. 2.3:

$$v_c = 6.19 y_1^{1/6} D_{50}^{1/3}$$

$$v_c = 6.19(0.1524m)^{\frac{1}{6}}(0.00045\ m)^{1/3} = 0.339\ m/s$$